RESEARCH ARTICLE

Characterization of the physiology and cell–mineral interactions of the marine anoxygenic phototrophic Fe(II) oxidizer *Rhodovulum iodosum* – implications for Precambrian Fe(II) oxidation

Wenfang Wu[1,2], Elizabeth D. Swanner[1], Likai Hao[3], Fabian Zeitvogel[3], Martin Obst[3], Yongxin Pan[2] & Andreas Kappler[1]

[1]Department of Geomicrobiology, Center for Applied Geosciences, University of Tuebingen, Tuebingen, Germany; [2]Key Laboratory of the Earth's Deep Interior, Institute of Geology and Geophysics, Chinese Academy of Sciences, Beijing, China; and [3]Environmental Analytical Microscopy, Center for Applied Geosciences, University of Tuebingen, Tuebingen, Germany

Correspondence: Andreas Kappler, Department of Geomicrobiology, Center for Applied Geosciences, University of Tübingen, Sigwartstrasse 10, D-72076 Tübingen, Germany. Tel.: +49-7071-2974992; fax: +49-7071-295059; e-mail: andreas.kappler@uni-tuebingen.de

Received 27 December 2013; revised 19 February 2014; accepted 28 February 2014. Final version published online 25 March 2014.

DOI: 10.1111/1574-6941.12315

Editor: Alfons Stams

Keywords
marine photoferrotroph; anoxygenic phototrophic Fe(II) oxidation; banded iron formations.

Abstract

Anoxygenic phototrophic Fe(II)-oxidizing bacteria (photoferrotrophs) are suggested to have contributed to the deposition of banded iron formations (BIFs) from oxygen-poor seawater. However, most studies evaluating the contribution of photoferrotrophs to Precambrian Fe(II) oxidation have used freshwater and not marine strains. Therefore, we investigated the physiology and mineral products of Fe(II) oxidation by the marine photoferrotroph *Rhodovulum iodosum*. Poorly crystalline Fe(III) minerals formed initially and transformed to more crystalline goethite over time. During Fe(II) oxidation, cell surfaces were largely free of minerals. Instead, the minerals were co-localized with EPS suggesting that EPS plays a critical role in preventing cell encrustation, likely by binding Fe (III) and directing precipitation away from cell surfaces. Fe(II) oxidation rates increased with increasing initial Fe(II) concentration (0.43–4.07 mM) under a light intensity of 12 μmol quanta $m^{-2}s^{-1}$. Rates also increased as light intensity increased (from 3 to 20 μmol quanta $m^{-2}s^{-1}$), while the addition of Si did not significantly change Fe(II) oxidation rates. These results elaborate on how the physical and chemical conditions present in the Precambrian ocean controlled the activity of marine photoferrotrophs and confirm the possibility that such microorganisms could have oxidized Fe(II), generating the primary Fe(III) minerals that were then deposited to some Precambrian BIFs.

Introduction

The geochemical cycling of iron (Fe) in terrestrial and marine environments is heavily influenced by microbial activity. Microorganisms gain energy from both Fe(III) reduction and Fe(II) oxidation (Bird *et al.*, 2011; Konhauser *et al.*, 2011). Iron-based metabolisms are spread throughout the bacterial and archaeal branches of the phylogenetic tree (Weber *et al.*, 2006) and may have been some of the earliest metabolisms on Earth (Vargas *et al.*, 1998). Anoxygenic photosynthesis using Fe(II) as an electron donor is thought to evolutionarily pre-date oxygenic photosynthesis (Xiong, 2006). Under anoxic conditions, so-called photoferrotrophs can couple the oxidation of Fe(II) to the reduction of bicarbonate using light energy (Ehrenreich & Widdel, 1994), with the stoichiometry:

$$HCO_3^- + 4Fe^{2+} + 10H_2O \rightarrow CH_2O + 4Fe(OH)_3 + 7H^+ \quad (1)$$

Photoferrotrophs were suggested to account for significant Fe(II) oxidation in oxygen-poor seawater that resulted in the deposition of mixed-valence Fe-rich sediments from Precambrian seawater (Konhauser *et al.*, 2002; Kappler *et al.*, 2005a; Posth *et al.*, 2008, 2013), examples of which include the banded iron formations (BIFs), deposited in the Archean to Paleoproterozoic (*c.* 3.5–1.8 Ga; Bekker *et al.*, 2010).

Previous physiological studies of three phylogenetically distinct freshwater photoferrotrophs (*Rhodobacter ferrooxidans* sp. strain SW2, *Chlorobium ferrooxidans* strain KoFox and *Thiodictyon* sp. strain F4) (Kappler & Newman, 2004; Hegler *et al.*, 2008; Schaedler *et al.*, 2009) have been used to assess the possibility that photoferrotrophs were involved in Fe(II) oxidation under anoxic conditions. Calculations using Fe(II) oxidation rates from a freshwater strain coupled to the physical and chemical characteristics of Archean seawater suggested that photoferrotrophs could drive the full oxidation of Fe(II) upwelling from deep, hydrothermal sources at rates consistent with those needed to explain deposition of Fe(III) to major Precambrian BIFs and supporting the role of photoferrotrophy in Fe(II) oxidation in anoxic Precambrian seawater (Kappler *et al.*, 2005a).

Despite the potential importance of photoferrotrophs to marine Fe(II) oxidation in the Precambrian, only one study to date has described the physiology of marine photoferrotrophs (Straub *et al.*, 1999). Yet the solution chemistry (e.g. chloride concentration) and (organic) ligands (e.g. presence of siderophores) that control the speciation and reactivity of iron in the ocean differ from freshwater. These factors might affect the rates of photosynthetic Fe(II) oxidation and the concomitant Fe(III) minerals formed. Furthermore, photoferrotrophs are phylogenetically diverse, and genes implicated in this process are not homologous among different isolates (Croal *et al.*, 2007), suggesting that the Fe(II) oxidation process could vary among distinct species. While laboratory examination of the Fe isotope fractionation and Fe(II) oxidation rates of some freshwater strains support the role of photoferrotrophic Fe(II) oxidation in the deposition of iron minerals to BIFs (e.g. Johnson *et al.*, 2003; Croal *et al.*, 2004; Kappler *et al.*, 2005a; Hegler *et al.*, 2008; Czaja *et al.*, 2013), constraining Fe(II) oxidation rates of a marine photoferrotroph might give additional insights about the role of anoxygenic photosynthesis in Fe(II) oxidation under conditions relevant to Precambrian BIF deposition.

Previous studies have provided the identity of a few genes and enzymes associated with anoxygenic photosynthetic Fe(II) oxidation (Croal *et al.*, 2007; Jiao & Newman, 2007). Despite this, our understanding is fragmented regarding, for example, why the often negatively charged cell surfaces do not become encrusted by the positively charged Fe(III) minerals formed during photosynthetic Fe (II) oxidation, as has been shown for other freshwater anaerobic Fe(II)-oxidizing strains (Kappler & Newman, 2004; Hegler *et al.*, 2008; Schaedler *et al.*, 2009). A low-pH microenvironment surrounding the cell surface during Fe(II) oxidation might prevent Fe(III) minerals from precipitating around the cells, circumventing cell encrustation (Schaedler *et al.*, 2009; Hegler *et al.*, 2010). Bacterially produced organic polymers were also suggested to be a strategy for photoferrotrophs to avoid encrustation by templating iron minerals during precipitation (Chan *et al.*, 2004; Miot *et al.*, 2009a) or by solubilizing Fe(III) through complexation (Schaedler *et al.*, 2009). Besides these strategies, modification of the cell surface charge has also been proposed (Schaedler *et al.*, 2009; Saini & Chan, 2013).

In the present study, growth and activity of the marine strain *Rhodovulum iodosum*, originally isolated by Straub *et al.* (1999), were examined at several initial Fe(II) concentrations and light intensities. Fe(II) oxidation in the presence of Si was also examined to simulate conditions of the Precambrian seawater saturated with respect to Si (Maliva *et al.*, 2005). By investigating the Fe(II) oxidation and Fe(III) mineral precipitation processes of the marine strain *R. iodosum* and comparing these results with the physiology of well-characterized freshwater strains (e.g. Hegler *et al.*, 2008; Miot *et al.*, 2009a), we enhance the knowledge on how Fe(II) oxidation and Fe(III) precipitation occur during microbial Fe(II) oxidation. Specifically, this study evaluates whether the cells of this marine strain become coated by the Fe(III) minerals precipitated during Fe(II) oxidation as it occurs in some anaerobic nitrate-reducing Fe(II)-oxidizing bacteria (Klueglein *et al.*, 2014). We also use our results to quantitatively re-evaluate whether marine photoferrotrophs could drive full oxidation of upwelling Fe(II) from anoxic waters in the Precambrian (Kappler *et al.*, 2005a).

Materials and methods

Strain source

The marine photoferrotroph *R. iodosum* was obtained from Deutsche Sammlung von Mikroorganismen und Zellkulturen (DSMZ), Germany (DSM 12328T). It was isolated from a mud flat of the Jadebusen (North Sea) (Straub *et al.*, 1999).

Culturing medium

The strain *R. iodosum* was routinely cultured using marine phototroph medium (20 g NaCl, 6.8 g $MgSO_4$*$7H_2O$, 1.5 g $CaCl_2$*$2H_2O$, 0.25 g NH_4Cl, 0.4 g KH_2PO_4, 0.09 g KBr, 0.66 g KCl in 1 L Millipore water). The medium was prepared in a Widdel flask and flushed with N_2/CO_2 (v/v, 90/10) after autoclaving. Sodium bicarbonate (22 mM) was used as the primary buffer, and the pH was adjusted to 6.80 with HCl or Na_2CO_3. As *R. iodosum* can only oxidize Fe(II) within a narrow pH range of 6.3–6.8 (Straub *et al.*, 1999), we chose the upper limit of the pH range (6.8) to simulate the circumneutral Archean seawater

(Hardie, 2003). Additions of trace elements included $FeCl_3$ solution (3 mg L^{-1}), selenium tungstate solution (0.4 g NaOH, 6 mg $Na_2SeO_3*5H_2O$, and 8 mg $Na_2WO_4*2H_2O$ in 1 L Millipore water), vitamin solution (1 mg biotin, 10 mg nicotinate, 5 mg aminobenzoic acid, 2.5 mg Ca-D(+) pantothenate, 25 mg pyridoxaine dihydrochloride, 5 mg thiaminium dihydrochloride, and 100 mg vitamin B_{12} in 100 mL Millipore water), and trace element solution (10 mL of 25% HCl, 2.86 g H_3BO_3, 0.5 g $MnCl_2*4H_2O$, 180 mg $ZnCl_2$, 36 mg $Na_2MoO_4*2H_2O$, 2 mg $CuCl_2*2H_2O$, 24 mg $NiCl_2*6H_2O$, 190 mg $CoCl_2*6H_2O$, and 1.5 g $FeCl_2*4H_2O$ in 1 L Millipore water) and were added to the basal medium at 1 mL per liter, while $Na_2S_2O_3$ solution (1 mM) was added at 0.5 mL per liter. Then, 25 mL of the medium was transferred to 58-mL serum bottles, and the headspace was flushed with H_2/CO_2 (v/v, 80/20) for 3 min before inoculation when H_2 served as the electron donor. When Fe(II) was the electron donor, a headspace of N_2/CO_2 was used. Cultures were incubated at 26° C and 12 μmol quanta $m^{-2}s^{-1}$ (600 lux) with a 40-W tungsten incandescent light bulb.

Growth on H_2

To determine the dependence of *R. iodosum* growth rates on light intensity, in cultures growing on H_2, the light intensity was varied from 3, 12 to 20 μmol quanta $m^{-2}s^{-1}$ (150, 600 and 1000 lux) by placing the tubes at different distances from the tungsten light bulb. Cells were incubated in 15-mL glass tubes (7.5 mL medium), and growth was monitored through optical density measurements at $OD_{660\ nm}$ on a spectrophotometer (Analytik Jena SPEKOL 1300). H_2/CO_2 was flushed through the headspace every other day during incubation.

Fe(II) oxidation and growth on Fe(II)

Fe(II) oxidation and growth of *R. iodosum* were determined by culturing *R. iodosum* in medium with various initial Fe(II) concentrations (0.5, 1, 1.5, 2, and 5 mM) under different light intensities (3, 6, 12, 16, and 20 μmol quanta $m^{-2}s^{-1}$) with a 40-W tungsten incandescent light bulb. To prepare Fe(II)-containing medium, 1 M anoxic sterile $FeCl_2$ stock solution was prepared and added to a basal medium (Hegler *et al.*, 2008). The gray greenish precipitates (likely siderite and vivianite) were filtered out (Millipore filter, 0.22 μm) in a glove box similar to the procedure in Hegler *et al.* (2008) but with two differences: the medium was filtered twice to completely remove the precipitates and the medium was incubated in the dark at 5° C for 24 h before each filtration to maximize removal of Fe phosphate and carbonate precipitates, due to decreased solubility of these phases at low temperature. Cells were pregrown using H_2 as an electron donor at 12 μmol quanta $m^{-2}s^{-1}$ to exponential stage and then about 1% of the log-phase inoculum was added to the Fe(II)-containing medium to yield a cell number of $\sim 1.5 \times 10^7$ cells mL^{-1}. This protocol ensured that reactive Fe mineral surfaces were not added from the inoculum. All experiments were set up in triplicates. Sterile controls contained all ingredients but no cells. Fe(II) oxidation rates determined at different light intensities and initial Fe(II) concentrations were fit to a Michaelis–Menten equation to determine V_{max} (maximum oxidation rate) and K_m (half-saturation light intensity/Fe(II) concentration) (Hegler *et al.*, 2008).

The effect of Si addition on Fe(II) oxidation was examined at 2 mM Fe(II). A Si stock solution (50 mM $NaSiO_3*9H_2O$) was prepared anoxically at 80° C and then added to the 2 mM Fe medium through a 0.2-μm filter to a final concentration of 2.2 mM to simulate proposed Precambrian seawater saturated with amorphous Si (Maliva *et al.*, 2005). An unpaired, two-tailed *t*-test at a 95% confidence interval was used to determine whether the Fe(II) oxidation rates obtained from triplicate experiments under one condition (e.g. with Si) were statistically significant from the average value obtained from a second set of experiments (e.g. without Si).

Fe(II) and total Fe analysis

Time-interval sampling for Fe(II) and total Fe quantification was conducted in an anoxic glove box (100% N_2). The culture suspension was dissolved anoxically with 6 M HCl or 1 M HCl (Porsch & Kappler, 2011) for total Fe and Fe(II) determination. Fe(II) concentrations were measured using the ferrozine assay (Stookey, 1970). Total Fe was determined after incubating the solution with the reducing agent hydroxylamine hydrochloride acid (10% wt/v, prepared in 1 M HCl) for 30 min, and the Fe(III) concentration was obtained by the difference between total Fe and Fe(II). The absorbance was read through a microtiter plate reader (Analytik Jena Flash Scan 550) at a wavelength of 562 nm.

Microscopy

Growth of *R. iodosum* at 4.07 mM Fe(II) and 12 μmol quanta $m^{-2}s^{-1}$ was quantified by fluorescent microscopic cell counts. For cell counts, a sample of the culture was first fixed with paraformaldehyde at a final concentration of 2.5% and incubated at 4° C until analysis. The fixed sample was then centrifuged for 10 min at 16 000 ***g***, and the pellet was re-suspended in a solution of ferrous ethylenediammonium sulfate (one part, 100 mM) and oxalic

acid (nine parts, 28 g L^{-1} ammonium oxalate and 15 g L^{-1} oxalic acid) for 10 min to dissolve the iron minerals. The cells were then suspended in a mixture of Tris buffer (nine parts) and sodium pyrophosphate (one part) and briefly sonicated to disperse cell aggregates. The dye Sytox Green (Invitrogen) was used to stain the cells, which were then filtered onto a black polycarbonate filter (Millipore, 0.22 μm). Cells were counted using a Leica DM5500B fluorescence microscope using the L5 filter. At least 40 image frames or a total of 1000 individual cells, respectively, were counted per sample.

For scanning electron microscopy (SEM) imaging, ~ 1 mL of culture was taken at the end of incubation, washed with Millipore water, and centrifuged. The pellet was then re-suspended in acetone, and one drop was loaded onto a sticky carbon pad mounted on an aluminum stub (both Plano GmbH, Wetzlar, Germany), and dried in a vacuum chamber (−0.9 bar). The sample was sputter-coated with 6–8 nm platinum (BAL-TEC SCD 005, BAL-TEC, Liechtenstein, 35 mm working distance, 30 mA, 60 s). A Leo Model 1450VP SEM (Carl Zeiss SMT AG, Germany) was operated at 7 kV and 6 mm working distance with a secondary electron (SE) detector.

To obtain more information about the cell–mineral associations of this strain, cell–mineral aggregates were analyzed using a confocal laser scanning microscope (CLSM; Leica SPE, Mannheim, Germany). Three different dyes were added to the sample sequentially in a glove box to stain DNA (SYTO® 9 green fluorescent nucleic acid stain, Molecular probes, Invitrogen), extracellular polymeric substances (EPS; wheat germ agglutinin, Alexa Fluor® 633 conjugate, Molecular probes, Invitrogen), and dissolved/complexed Fe(III) (Yang *et al.*, 2012). Excitation lasers with wavelengths of 488, 561, and 635 nm were used to collect fluorescence signals at wavelength ranges of 490–510, 579–620, and 640–700 nm for DNA, Fe(III), and EPS probes, respectively. The reflection signal of the 488 nm laser was used to detect mineral particles. The dye combinations and wavelengths of fluorescence were optimized to avoid fluorescence overlap. Spatial correlations of these signals were analyzed with IMAGEJ (Abràmoff *et al.*, 2004) using a custom-made plugin to generate scatterplots of fluorescent signals. As a measure of correlation, we calculated the root-mean-square error (RMSE) of the reduced major axis regression line. To make RMSE values comparable, units were normalized to the maximum signal of each channel.

Mineralogical analyses

The intermediate (after 42% of Fe(II) had been oxidized) and final mineral products of Fe(II) oxidation by *R. iodosum* at 4.07 mM Fe(II) and 12 μmol quanta $m^{-2}s^{-1}$ were collected for micro X-ray diffraction (μXRD). We prepared the samples both anoxically and oxically to discern if products were stable with respect to subsequent oxygen exposure. Samples were washed with DI water three times to remove residual salts, air-dried, and loaded to a Si single-crystal silicon wafer. For anoxic preparation, all the sampling, washing, drying, and loading steps were conducted in an anoxic glove box, and the slide was kept anoxic until measurement. Data were collected with a Bruker D8 Discover XRD instrument (Bruker, Germany) equipped with a Co Kα X-ray tube (λ = 0.17902 nm, 30 kV, 30 mA) and GADDS area detector (Berthold *et al.*, 2009). Mineral phases were identified using the International Center for Diffraction Data (ICDD) database.

Results

Effects of initial Fe(II) concentration on Fe(II) oxidation rates

Due to filtration of the medium before use, ~ 6–30% of the initially added Fe(II) (that was precipitated as Fe(II) carbonate and Fe(II) phosphate) was removed so that the initial Fe(II) concentrations used in experiments were 0.43, 0.70, 1.26, 1.51, and 4.07 mM. Fe(II) oxidation was followed over time at all of these Fe(II) concentrations at a light intensity of 12 μmol quanta $m^{-2}s^{-1}$ and an initial cell number of ~ 1.5×10^7 cells mL^{-1}. *Rhodovulum iodosum* showed a lag phase during which the Fe(II) concentration was nearly unchanged, before it started oxidizing Fe(II). The lag time increased with the initial Fe(II) concentration, from 1 to 3 days at 0.4–1 mM Fe(II) to 7–9 days at 1.2–5 mM Fe(II). A lag phase of ~ 8 days was also observed for this strain at 10 mM Fe(II) (Straub *et al.*, 1999). As the experiments were performed at similar light intensities as the cultures used for inoculation, the lag phase observed stems either from adaptation to Fe(II) or, supported by the fact that the lag phase increases with Fe(II) concentration, from Fe(II) toxicity effects as described before for anaerobic Fe(II)-oxidizing bacteria (Bird *et al.*, 2013). Following the lag phase, Fe(II) was oxidized completely (> 97%) during further incubation. Fe(II) oxidation rates were calculated by linear regression of the steepest part of the Fe(II) vs. time plots. The average of three parallel bottles resulted in an Fe(II) oxidation rate of 1.27 ± 0.15 mM day^{-1} at 4.07 mM initial Fe(II), which decreased to 0.15 ± 0.02 mM day^{-1} at 0.43 mM Fe(II) (Fig. 1a). Si addition to the 1.51 mM Fe (II) medium had no significant effect on the Fe(II) oxidation rate (0.73 ± 0.01 vs. 0.69 ± 0.04 mM day^{-1} with and without Si; *P*-value = 0.2954; Fig. 1a), only that the onset of Fe(II) oxidation by *R. iodosum* was delayed by

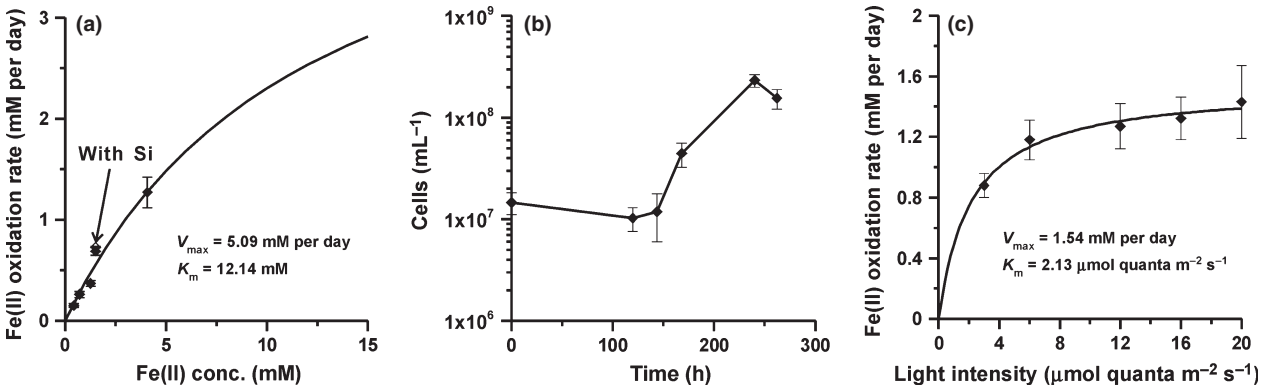

Fig. 1. Fe(II) concentration- and light intensity-dependent Fe(II) oxidation by *Rhodovulum iodosum*. (a) Fe(II) oxidation rate vs. initial Fe(II) concentration at a light intensity of 12 μmol quanta $m^{-2}s^{-1}$; the open symbol represents the medium with 2.2 mM Si. (b) Cell growth at 4.07 mM initial Fe(II) under light intensity of 12 μmol quanta $m^{-2}s^{-1}$ with 1% inoculation. (c) Fe(II) oxidation rate vs. light intensity with 4.07 mM initial Fe(II). The V_{max} and K_m were determined by fitting the Fe(II) oxidation rates at different Fe(II) concentrations and light intensities to a Michaelis–Menten equation (a and c).

~ 48 h compared to that with no Si. No Fe(II) oxidation was observed in an abiotic (uninoculated) control incubated under identical conditions.

Microbial growth and pH change during phototrophic Fe(II) oxidation by *R. iodosum*

Growth of *R. iodosum* in experiments with 4.07 mM initial Fe(II) was monitored using fluorescence microscopic cell counts (Fig. 1b). Cell numbers dropped slightly from 1.5×10^7 to 1.0×10^7 cells mL^{-1} during the lag phase. Then, cells increased quickly, by more than one order of magnitude during the Fe(II) oxidation stage, reaching a maximum of 2.3×10^8 cells mL^{-1} at 240 h. This yields a cell number-normalized Fe(II) oxidation rate of 4.7×10^{-16} mol Fe(II)/h per cell, significantly faster than the rate we calculated for the freshwater strain *R. ferrooxidans* SW2 at saturated light intensity with 4 mM initial Fe(II) (3.8×10^{-17} mol Fe(II)/h per cell) from data in Hegler *et al.* (2008).

Following Fe(II) oxidation, the pH of the medium decreased from the initial neutral pH (6.80) to 6.51 ± 0.06. Precipitation of Fe(III) following oxidation is accompanied by proton generation, according to Eqn.(1), which likely leads to the observed pH decrease. The pH for the abiotic control stayed constant during the time course of the experiments (6.80 ± 0.04).

Effects of light intensity on Fe(II) oxidation rates

Growth experiments were also conducted at different light intensities (3, 6, 12, 16, and 20 μmol quanta $m^{-2}s^{-1}$) at 4.07 mM initial Fe(II) to examine the dependence of Fe(II) oxidation by *R. iodosum* on light intensity. The highest and lowest light intensities (3 and 20 μmol quanta $m^{-2}s^{-1}$) induced a lag phase of ~ 12 days with no significant Fe(II) oxidation prior to rapid Fe(II) oxidation, and the lag time was longer than that observed at intermediate light intensities (about 8–10 days at 6, 12, and 16 μmol quanta $m^{-2}s^{-1}$). Higher light intensities resulted in an increase in the Fe (II) oxidation rate once the strain started oxidizing Fe (II). The Fe(II) oxidation rate of *R. iodosum* at 3 μmol quanta $m^{-2}s^{-1}$ was 0.88 ± 0.08 mM day^{-1}, which increased to 1.43 ± 0.24 mM day^{-1} at 20 μmol quanta $m^{-2}s^{-1}$ (Fig. 1c). The rate did not level off at 20 μmol quanta $m^{-2}s^{-1}$, which suggests that Fe(II) oxidation rate of *R. iodosum* should continue to increase above the highest applied light intensity (20 μmol quanta $m^{-2}s^{-1}$; Fig. 1c). The extent of Fe(II) oxidation was always the same at the light intensities tested (> 97%).

Effects of light intensity on growth rates with H_2 as electron donor

Growth rate dependence on light intensity was examined by growing *R. iodosum* at 3, 12, and 20 μmol quanta $m^{-2}s^{-1}$ with H_2 as the sole electron donor. The cell-specific growth rate (μ; day^{-1}) increased with light intensity, but did not reach a maximum even at the highest light intensities we considered here (20 μmol quanta $m^{-2}s^{-1}$; Fig. 2). The fastest cell-specific growth rate was 0.98 day^{-1}.

Microscopic analysis of cell–mineral aggregates

The cell–mineral aggregates of Fe(III) minerals precipitated in *R. iodosum* cultures were examined after complete

Fe(II) oxidation by SEM (Fig. 3). Individual cells were 1–2 μm long and associated with but not coated by or encrusted in mineral particles of 100–300 nm diameter.

We conducted confocal laser scanning microscopic analysis of wet samples to further confirm the native associations of cell–EPS–mineral aggregates (Fig. 4). Imaging the cell–mineral aggregates in a hydrated state obviates artifacts such as agglomeration and cell lysis encountered during drying of the samples for SEM. The fluorescence signals of the Fe(III)-specific fluorescent probe and of the lectin-conjugate binding to EPS are co-localized (Fig. 4b, c, and e), supported by the RMSE values after reduced major axis fitting of 2D scatterplots of the signal intensities from each of the fluorescence channels (Fig. 5a). This correlation suggests that the Fe (III) is closely associated with organic structures like EPS. The EPS signal is also co-localized with the reflection (mineral) signal (Fig. 4c–e), as determined by correlations in 2D scatterplots (Fig. 5b). The signal of the DNA-binding dye (Fig. 4a), indicating cells, was spatially separated from the fluorescence of the lectin-conjugate EPS dye and the mineral reflection signal (Fig. 4c–e; Fig. 5c and d), indicating that cells were not surrounded or encrusted by EPS or minerals, confirming our SEM results.

Mineralogy

The identity of the intermediate and final mineral products of Fe(II) oxidation was examined by μ-XRD. Samples prepared for μ-XRD under anoxic and oxic conditions showed little difference in the diffraction peak positions (data not shown) confirming that the minerals produced by *R. iodosum* are not sensitive to subsequent oxidation and likely composed of only Fe(III). The μ-X-ray diffractogram of the intermediate phase did not have any reflections corresponding to a crystalline mineral phase, suggesting a poorly crystalline or amorphous phase (Fig. 6a). More crystalline phases of goethite (α-FeOOH) minerals were formed, with minor fractions of lepidocrocite (γ-FeOOH), at the end of incubation (Fig. 6b). No Fe phosphate minerals (e.g. vivianite) were detected by μ-XRD, although a significant concentration of phosphate was present in the medium after double filtration (~ 40–60 μM).

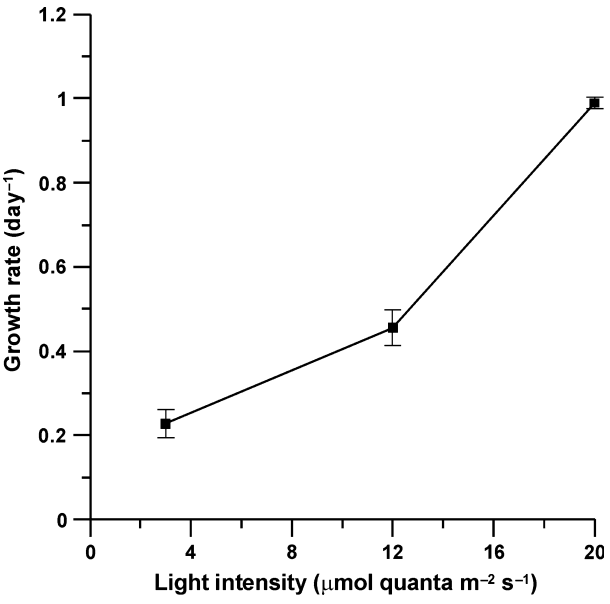

Fig. 2. Light intensity-dependent cell growth rates determined with H_2 as electron donor. Light intensity was varied by changing the distance between the culturing tubes and the tungsten light bulb.

Discussion

Fe(III) precipitates formed by *R. iodosum*

At circumneutral pH (6.80) in the growth experiments, the Fe(III) formed as a result of Fe(II) oxidation is poorly

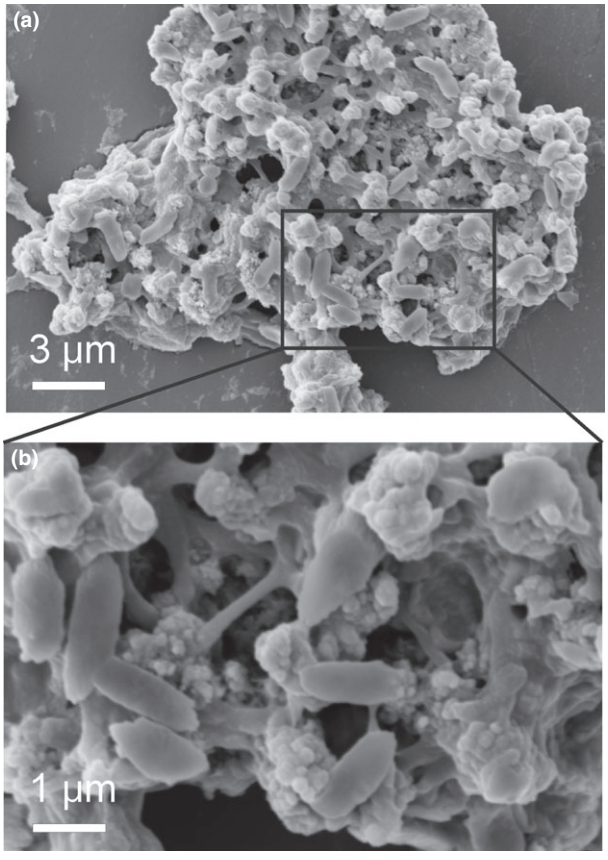

Fig. 3. SEM images of the cell–mineral aggregates formed by *Rhodovulum iodosum* when oxidizing 4.07 mM Fe(II) at a light intensity of 12 μmol quanta $m^{-2}s^{-1}$; (b) is an enlarged image of (a).

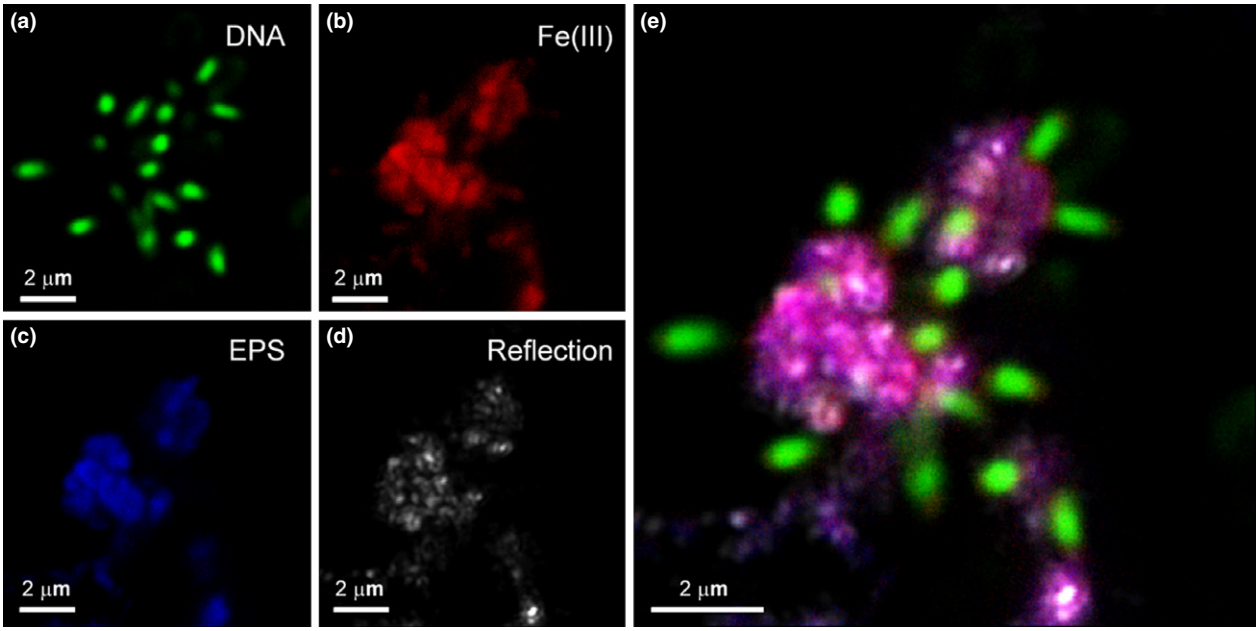

Fig. 4. CLSM 2D images of the cell–mineral aggregates of *Rhodovulum iodosum* cultivated with 4.07 mM initial Fe(II) at a light intensity of 12 μmol quanta $m^{-2}s^{-1}$. The green, red, blue, and gray color correspond to DNA (a), Fe(III) (b), EPS (c), and reflection signal (d), while e shows an overlay of the images a, b, c, and d.

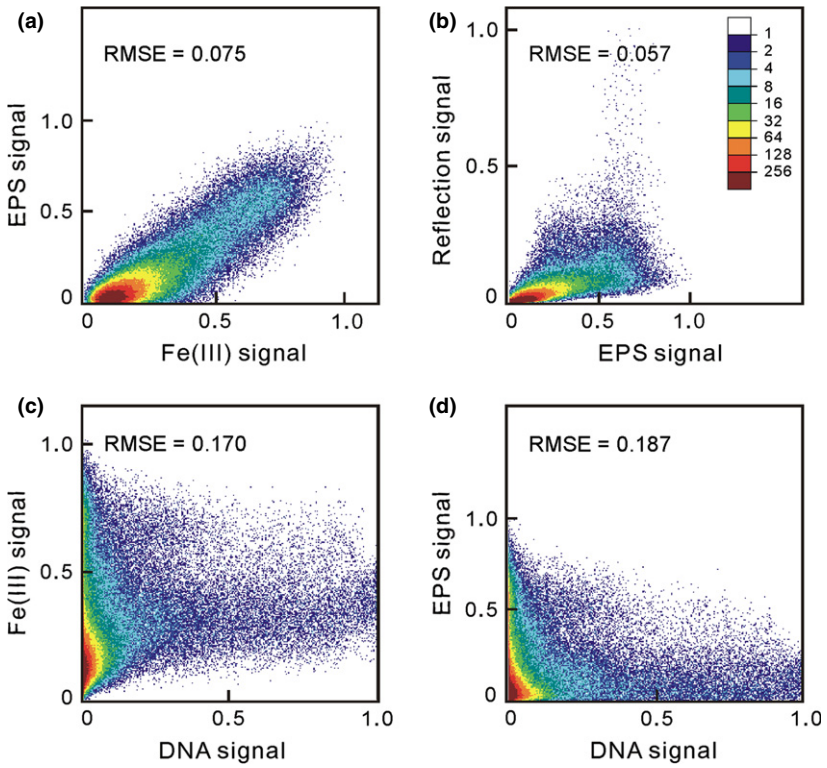

Fig. 5. Scatterplots of EPS and Fe(III) signals (a), reflection and EPS signals (b), Fe(III) and DNA signals (c), and EPS and DNA signals (d). The color scale represents the frequency of occurrence. Units are normalized to the maximum signal for each channel. RMSE represents the root-mean-square error value obtained from reduced major axis regression of the scatterplots.

soluble and should readily precipitate as Fe(III) (oxyhydr) oxide minerals. In the initial report on the cultivation of *R. iodosum*, ferrihydrite formation was observed when 60–70% of Fe(II) was oxidized (Straub *et al.*, 1999). Poorly crystalline Fe minerals without obvious diffraction peaks were detected at the initial stage during Fe(II)

oxidation in our experiments, likely ferrihydrite (Fig. 6a). These mineral particles were of a comparable size to the Fe minerals formed by freshwater photoferrotrophs (Fig. 3; Miot *et al.*, 2009a; Schaedler *et al.*, 2009). Goethite was the dominant final Fe(III) phase at the end of incubation (Fig. 5b). This suggests that once ferrihydrite forms, it is not stable and readily transformed to more crystalline goethite during further incubation. Similar transformation of ferrihydrite to goethite was also observed with the freshwater photoferrotroph *R. ferrooxidans* SW2 (Kappler & Newman, 2004), probably suggesting a common aging effect, or more likely, that the presence of Fe(II) induces the transformation of ferrihydrite to goethite via recrystallization (Hansel *et al.*, 2003). Although no magnetite peaks were observed in our μ-XRD analysis of the final minerals, Straub *et al.* (1999) did report minor magnetite formation during Fe(II) oxidation by *R. iodosum*.

In aqueous environments, Fe(III) resulting from Fe(II) oxidation is commonly precipitated as goethite and lepidocrocite minerals, consistent with the final products of our experiments. With increasing bicarbonate concentrations, goethite formation is favored (Carlson & Schwertmann, 1990; Larese-Casanova *et al.*, 2010), and at HCO_3^- saturation, only goethite minerals form (Carlson & Schwertmann, 1990). In this study, 22 mM bicarbonate buffer was used, which favors the precipitation of the goethite, although saturation of HCO_3^- (57 mM), estimated by linear extrapolation according to Carlson & Schwertmann (1990), was not reached in the growth medium. Thus, co-existence of goethite and lepidocrocite minerals as we observed is expected. Besides inorganic ligands like HCO_3^-, the average Fe(II) oxidation rate (AOR) also influences the identity of the final Fe(III) products. Carlson & Schwertmann (1990) suggested an equation for the mineralogical composition of final Fe (III) products using the HCO_3^- concentration and AOR at pH 7:

$$\mathrm{Lp}/(\mathrm{Lp}+\mathrm{Goe}) = 0.50 - 0.0067 * [\mathrm{HCO_3^-}] + 0.167\mathrm{AOR} \quad (2)$$

The amount of lepidocrocite estimated this way should be no more than 35% of the final Fe(III) products during Fe(II) oxidation by *R. iodosum* at 4.07 mM Fe(II). This is consistent with our μ-XRD data showing formation of both goethite and lepidocrocite at the end of incubation (Fig. 6b).

The influence of other anions like phosphate on the Fe (III) minerals formed during microbial Fe(II) oxidation has been discussed for other strains. A disordered or amorphous Fe(III) phosphate was observed during Fe(II) oxidation by *Acidovarax* sp. strain BoFeN1 at total phosphate concentration of 0.2 and 1 mM (Miot *et al.*, 2009b; Larese-Casanova *et al.*, 2010). Yet in our current medium, the phosphate concentration is quite low (~ 40–60 μM) after double filtration, and no Fe(III) phosphate mineral was detected. More likely, μM concentrations of phosphate may promote the formation of less crystalline phases (i.e. ferrihydrite) during initial oxidation (Swanner *et al.*, 2011).

How does the marine photoferrotroph *R. iodosum* avoid cell encrustation?

Goethite, with its high point of zero charge, results in positively charged minerals at the near neutral pH range in our experiments. Therefore, goethite is expected to encrust cells, as cell surfaces are often negatively charged. However, CLSM images show that the cells are not encrusted by the Fe(III) minerals precipitated (Fig. 4), which is similar to the case for freshwater photoferrotrophs (Hegler *et al.*, 2008). An ability to avoid encrustation seems to characterize photoferrotrophs generally, in contrast to the nitrate-reducing Fe(II) oxidizers, which become encrusted by Fe(III) minerals produced during Fe (II) oxidation (Kappler *et al.*, 2005b; Klueglein *et al.*, 2014), which may hinder diffusion of nutrients and

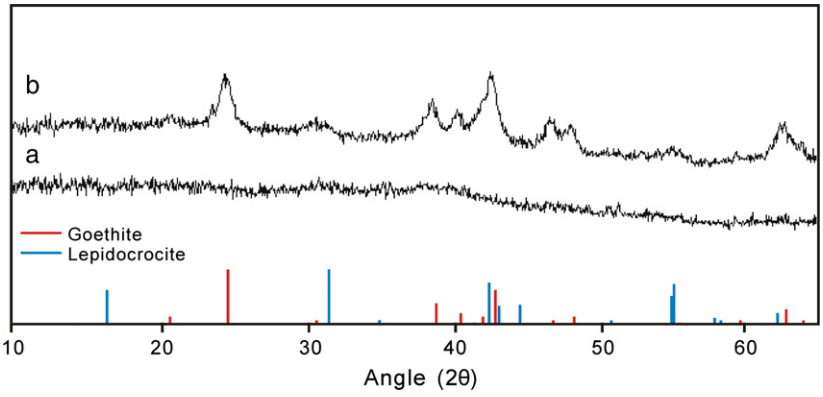

Fig. 6. Micro-X-ray diffraction data of the intermediate (a) and final mineral products (b) formed by *Rhodovulum iodosum* grown photoautotrophically with 4.07 mM Fe(II) at a light intensity of 12 μmol quanta $m^{-2}s^{-1}$. The intermediate mineral products were collected after ~ 42% of Fe(II) was oxidized. Poorly crystalline minerals formed initially, which transformed to more crystalline goethite minerals with minor fractions of lepidocrocite in the final mineral phase.

metabolites to the cell and waste products away from cell (Chan *et al.*, 2009).

The strategy of how cells avoid encrustation varies for different types of Fe(II)-oxidizing bacteria. For example, during microaerophilic Fe(II) oxidation, cells sometimes produce organic stalks or sheaths that bind Fe(III) minerals as they form (Emerson & Revsbech, 1994; Chan *et al.*, 2004; Hallberg & Ferris, 2004). Formation of soluble or colloidal Fe(III) compounds by lithotrophic aerobic Fe(II)-oxidizing bacteria was observed in gradient tubes where Fe(II)-oxidizing bacteria are grown in opposing gradients of O_2 and Fe(II) (Sobolev & Roden, 2001; Swanner *et al.*, 2011). For freshwater anoxygenic photoferrotrophs like *R. ferrooxidans* SW2, Fe(II) oxidation was suggested to occur in the periplasm (Croal *et al.*, 2007; Jiao & Newman, 2007), yet it was also suggested that these freshwater strains avoid encrustation or precipitation of Fe(III) minerals within the periplasm by generating local acidic environments to maintain Fe(III) as a soluble species until it diffuses away from the cell surface (Schaedler *et al.*, 2009; Hegler *et al.*, 2010).

We were interested in finding out whether our results can shed any light on how photoferrotrophs avoid cell encrustation during Fe(II) oxidation at near neutral pH (6.80). To this end, we used a fluorescent dye that binds to dissolved Fe(III) (i.e. ligand bound; complexed), but not to Fe(III) present in solid phase (i.e. minerals; Hao *et al.*, 2013). CLSM images (Fig. 4) show the presence of Fe(III) species that are spatially co-localized with EPS and reflection signals, away from the cell surface. The high correlation between EPS and Fe(III) signals (Fig. 5a), similar to what was observed in the freshwater photoferrotroph *R. ferrooxidans* SW2 (Miot *et al.*, 2009a), reveals that in addition to precipitation as Fe(III) minerals, a second fate for Fe(III) is binding to the EPS. Furthermore, pixels for complexed Fe(III) do not correlate with the DNA signal (Fig. 5c), which implies that the Fe(III) is not associated with the cells. The DNA and EPS signals were also spatially separated (Fig. 5d), but the EPS and reflection signals are correlated (Fig. 5b). All these likely point to the role of organic polymers in preventing cell encrustation, possibly via the binding of Fe(III) as a complexed phase that is detectable with an Fe(III)-binding dye and the ultimate precipitation of Fe(III) as minerals away from the cell surface.

Extracellular polymeric substances, thought to be dominantly polysaccharides based on high affinities for lectin probes, are excreted by both microaerophilic Fe(II)-oxidizing bacteria and photoferrotrophs (Miot *et al.*, 2009a; Chan *et al.*, 2011). Several studies have invoked the excretion of EPS, either as structural fibrils or as amorphous material, as a mechanism for preventing encrustation by Fe(III) minerals (Emerson & Ghiorse, 1993; Chan *et al.*, 2004, 2011; Miot *et al.*, 2009a; Schaedler *et al.*, 2009), by incorporating Fe(III) directly into the structure of the EPS (Chan *et al.*, 2011). The molecular interactions of Fe (III) when bound to a synthetic polymer indicate that Fe (III) is complexed by carboxyl groups, but that such bonds are not stable over timescales of weeks, and that Fe (III) will over time be precipitated as Fe(III) minerals (Chan *et al.*, 2009). Thus, our data are consistent with excretion of EPS as a strategy by *R. iodosum* and perhaps other photoferrotrophs to complex Fe(III) produced at or near the cell surface, preventing encrustation and delaying mineral formation. However, these models generally require direct contact between the cell and the EPS. The ~ 1 μm distance between cells of *R. iodosum* and the mineral–EPS–Fe(III) (Fig. 4) along with the lack of cell encrustation we observed is paradoxical to this model. The results seemingly require transportation of the EPS–Fe(III) phase away from the cell and subsequent precipitation and possible nucleation of further Fe(III) minerals (e.g. Schaedler *et al.*, 2009; Chan *et al.*, 2011). EPS is a term used to describe compositionally and functionally different polysaccharides, some of which are known to be soluble or mobile (Ramesh *et al.*, 2006), and it has been suggested that the solubility of the EPS excreted by cells changes during growth phases. For example, the EPS produced by cyanobacterium *Microcystis aeruginosa* was tightly bound to the cells during exponential growth stage, but released as soluble or loosely bound EPS at stationary and decay phase (Xu *et al.*, 2013). Although time-resolved microscopy would be needed to validate this model for *R. iodosum*, we suggest that cells may exploit the composition and/or solubility of EPS to transport complexed Fe(III) and precipitate away from the cells, thus avoiding cell encrustation.

The secretion of EPS may have consequences for the fate of Fe(III) minerals, once deposited to sediments such as BIFs. Cellular and extracellular organic carbon could be used by Fe(III)-reducing microorganisms as an electron donor for reduction of poorly crystalline Fe(III) minerals, generating secondary Fe(II) minerals (Konhauser *et al.*, 2005). Alternatively, abiotic reduction of Fe(III) minerals with organic carbon could also contribute to secondary Fe(II) mineral formation during diagenesis at increased temperatures and pressures (Koehler *et al.*, 2013; Posth *et al.*, 2013). In fact, it is likely that siderite ($FeCO_3$) in BIFs is commonly formed from either or both of these processes (Reinhard & Planavsky, 2011). For either of these reactions, the ability of organic carbon and the crystallinity of Fe(III) minerals should control the extent of Fe(III) reduction (Hansel *et al.*, 2004; Posth *et al.*, 2013). Therefore, an important consideration in determining the contribution of different types of

biomass generated through Fe(II) oxidation to either the organic content or secondary Fe(II) mineral formation in BIFs may be the reactivity of EPS toward microbial or thermogenic Fe(III) reduction.

Rates of Fe(II) oxidation by *R. iodosum* depending on light intensities – relevance for the activity of marine photoferrotrophs in modern environments

Rhodovulum iodosum can oxidize Fe(II) over a range of light intensities (3–20 μmol quanta $m^{-2}s^{-1}$, and likely higher) at up to 4.07 mM initial Fe(II). Light intensity within sediments of mud flats in the North Sea, from which this organism was isolated, does not exceed 100 μmol quanta $m^{-2}s^{-1}$ and is probably much lower (Billerbeck *et al.*, 2007). Therefore, the light intensities we investigated are within the range experienced by this organism in the environment. The trend of increasing Fe(II) oxidation rates with higher light intensities was also observed for freshwater photoferrotroph strains, and fit a Michaelis–Menten equation, indicating that the reaction rate is limited by how much light the photosystems of individual strains are able to absorb (Hegler *et al.*, 2008). Light saturation of Fe(II) oxidation by purple nonsulfur bacterium *R. ferrooxidans* SW2 and purple sulfur bacterium *Thiodictyon* sp. strain F4 was 8 and 16 μmol quanta $m^{-2}s^{-1}$ (400 and 800 lux), respectively, while for the green sulfur strain KoFox, Fe(II) oxidation rates saturated below 150 lux (Hegler *et al.*, 2008). For the marine strain purple nonsulfur bacterium *R. iodosum*, Fe(II) oxidation does not reach saturation even at light intensity of 20 μmol quanta $m^{-2}s^{-1}$ (1000 lux; Fig. 1c), indicating an adaptation to higher light conditions. This is consistent with the purple bacteria having higher light saturation than green sulfur bacteria (Overmann & Garcia-Pichel, 2000). We estimated that the maximum Fe(II) oxidation rate is 1.54 mM day^{-1} for *R. iodosum*, and the half maximum Fe (II) oxidation rate is reached at 2.13 μmol quanta $m^{-2}s^{-1}$ (106 lux), determined by iterating the Michaelis–Menten fit of our data in Fig. 1c with different K_m and V_{max} values until the highest correlation coefficient was achieved. The Fe (II) oxidation rate of *R. iodosum* is comparable to that of freshwater purple bacteria *Thiodictyon* strain F4 at similar light intensity, for example, 1.27 vs. 1.5 mM day^{-1} at 12 μmol quanta $m^{-2}s^{-1}$ (Croal *et al.*, 2004), indicating that oxidation rates among the purple bacteria may be generally similar at the same light intensities.

Potential role of marine photoferrotrophs in Fe cycling on early Earth

Although most photoferrotrophs have been isolated from sediments, they are still relevant to understanding the possible constraints on photoferrotrophy as a mechanism for Fe(II) oxidation in Precambrian oceans, which likely contributed to the deposition of BIFs. Based on evidence that Fe(II) was restricted to deeper waters in Precambrian oceans, it is thought that photoferrotorphs lived below a mixed layer, where light intensity was attenuated to perhaps less than 10% of the 600 μmol quanta $m^{-2}s^{-1}$ experienced on a sunny day at the water surface (Kappler *et al.*, 2005a and references therein). In fact, physical, chemical and ecological stratification are observed in a modern ferruginous lake, where putative photoferrotrophs live below 100 m depth at light intensities below 1 μmol quanta $m^{-2}s^{-1}$ (Crowe *et al.*, 2008). Our data validate that photoferrotrophy is still a viable metabolism at such low-light levels.

Porewater Fe(II) concentration in North Sea sediments, where *R. iodosum* was isolated, can reach 60–100 μM (Slomp *et al.*, 1997), similar to the Fe(II) concentration range estimated for anoxic Precambrian seawater in equilibrium with calcite and siderite (40–120 μM; Canfield, 2005). We therefore investigated growth of *R. iodosum* under a range of Fe(II) concentrations (0.43–4.07 mM), similar to those considered for some freshwater photoferrotrophs (Hegler *et al.*, 2008). Although our tested Fe(II) concentrations are still significantly higher than those estimated for Precambrian oceans, by utilizing a range we observed how Fe(II) oxidation rates respond to changing Fe(II) concentrations. Indeed, the Fe(II) oxidation rate by *R. iodosum* shows a Fe(II) concentration dependence. As the initial Fe(II) concentration decreased from 4.07 mM to 0.43 mM, the Fe(II) oxidation rate decreased by nearly one order of magnitude. In contrast, no clear Fe(II) oxidation rate dependence on Fe(II) concentration was observed previously for freshwater photoferrotrophs (Hegler *et al.*, 2008). Our data imply that substrate saturation of an enzyme controls the reaction rate (i.e. Michaelis–Menten kinetics; Fig. 1a), consistent with the activity of putative Fe oxidoreductases involved in the transfer of electrons from Fe(II) into the photosystems of the photoferrotroph *R. ferrooxidans* SW2 (Saraiva *et al.*, 2012). Importantly, *R. ferrooxidans* SW2 is the freshwater equivalent of the closely related *R. iodosum* (Straub *et al.*, 1999), and it is feasible that molecular mechanisms of Fe (II) oxidation may function similarly in these strains. Furthermore, at the same initial Fe(II) concentration, the Fe(II) oxidation rate by the marine photoferrotroph *R. iodosum* is comparable to that of freshwater strain *R. ferrooxidans* SW2 (e.g. 0.69 vs. ~ 0.60 mM day^{-1} at ~ 2 mM Fe(II); Hegler *et al.*, 2008).

The maximum Fe(II) oxidation rate predicted by a Michaelis–Menten fit of our data (Fig. 1a) should occur at concentrations above 10 mM Fe(II). Although the initial study detailing isolation of *R. iodosum* reported

robust growth at 10 mM Fe(II), we had difficulty cultivating the strain at these Fe(II) concentrations (data not shown). Although physiological fitness may have decreased over years of laboratory cultivation, it is possible that other factors limit putative Fe oxidoreductases from achieving their maximum rate. Recently, Bird *et al.* (2013) described the toxic effects of Fe(II) and Cu(II) on the photoferrotroph *Rhodopseudomonas palustris* TIE-1 under anoxic conditions. They noted that trace contamination of Cu in stocks of Fe(II) was enough to cause toxicity. Our medium with ~ 5 mM Fe(II) contains ~ 0.8 μM Cu (E.D. Swanner, unpublished data), much higher concentrations than were needed to affect growth of *R. palustris* TIE-1, implying an Fe(II)–Cu toxicity could explain the reduced growth we observed at 10 mM Fe(II).

Based on the Fe(II) oxidation rate of *R. ferrooxidans* SW2, Kappler *et al.* (2005a) suggested that anoxygenic photoferrotrophs could fully oxidize the Fe(II) upwelling from anoxic deep waters in the Precambrian ocean, despite limited light penetration below a wind-mixed layer. In the present study, we showed that the Fe(II) oxidation rate of marine photoferrotroph *R. iodosum* is dependent not only on light intensity, but also on initial Fe(II) concentration (Fig. 1). The calculations of Kappler *et al.* (2005a) utilized data from experiments with photoferrotrophs grown at ~ 5 mM Fe(II), a full order of magnitude higher than Fe(II) concentrations they cite for anoxic deep waters. *Rhodovulum iodosum* oxidizes 0.15 mM Fe(II) day^{-1} at 0.43 mM Fe(II) and 12 μmol quanta $m^{-2}s^{-1}$. Reasonable Fe(II) oxidation rates for photoferrotrophs living beneath a wind-mixed layer in anoxic waters may therefore be slower than suggested by Kappler *et al.* (2005a), given the effects of both light intensity and Fe(II) concentrations. Therefore, photoferrotrophs would need to extend to at least 50 m below the mixed layer rather than 17.6 m suggested by Kappler *et al.* (2005a), to account for complete oxidation of upwelling Fe(II) at the cell densities they suggested. Importantly, anoxygenic photosynthetic populations do inhabit intervals of ~ 50 m below the mixed layer in modern anoxic ferruginous and sulfidic water columns (Repeta *et al.*, 1989; Crowe *et al.*, 2008), suggesting such a scenario is reasonable. Finally, we have shown that Si addition does not affect the average Fe (II) oxidation rate of *R. iodosum*, and oceans at saturation with amorphous Si in the Precambrian should not have hindered the ability of photoferrotrophs to oxidize Fe(II).

Acknowledgements

We thank Nikolas Hagemann for help with SEM sample preparation and imaging, Jianli Li for providing the Fe (III) probe used in CLSM, and James Byrne for μXRD measurements. This study was supported by the European Research Council under the European Union's Seventh Framework Programme (FP/2007–2013)/ERC Grant, Agreement n. 307320 – MICROFOX. Additional funding came from CAS/SAFEA International Partnership Program for Creative Research Teams (KZCX2-YW-T10), the DFG Emmy-Noether program to MO (OB 362/1-1), NSFC (No. 40821091 and 20972124), and an NSF International Research Fellowship to EDS.

References

Abràmoff MD, Magalhães PJ & Ram SJ (2004) Image processing with IMAGEJ. *Biophotonics Int* **11**: 36–42.

Bekker A, Slack JF, Planavsky N, Krapez B, Hofmann A, Konhauser KO & Rouxel OJ (2010) Iron formation: the sedimentary product of a complex interplay among mantle, tectonic, oceanic, and biospheric processes. *Econ Geol* **105**: 467–508.

Berthold C, Bjeoumikhov A & Brügemann L (2009) Fast XRD^2 microdiffraction with focusing X-ray microlenses. *Part Part Syst Charact* **26**: 107–111.

Billerbeck M, Røy H, Bosselmann K & Huettel M (2007) Benthic photosynthesis in submerged Wadden Sea intertidal flats. *Estuar Coast Shelf Sci* **71**: 704–716.

Bird LJ, Bonnefoy V & Newman DK (2011) Bioenergetic challenges of microbial iron metabolisms. *Trends Microbiol* **19**: 330–340.

Bird LJ, Coleman ML & Newman DK (2013) Iron and copper act synergistically to delay anaerobic growth of bacteria. *Appl Environ Microbiol* **79**: 3619–3627.

Canfield DE (2005) The early history of atmospheric oxygen: homage to Robert M. Garrels. *Annu Rev Earth Planet Sci* **33**: 1–36.

Carlson L & Schwertmann U (1990) The effect of CO_2 and oxidation rate on the formation of goethite versus lepidocrocite from an Fe (II) system at pH 6 and 7. *Clay Min* **25**: 65–71.

Chan CS, De Stasio G, Welch SA, Girasole M, Frazer BH, Nesterova MV, Fakra S & Banfield JF (2004) Microbial polysaccharides template assembly of nanocrystal fibers. *Science* **303**: 1656–1658.

Chan CS, Fakra SC, Edwards DC, Emerson D & Banfield JF (2009) Iron oxyhydroxide mineralization on microbial extracellular polysaccharides. *Geochim Cosmochim Acta* **73**: 3807–3818.

Chan CS, Fakra SC, Emerson D, Fleming EJ & Edwards KJ (2011) Lithotrophic iron-oxidizing bacteria produce organic stalks to control mineral growth: implications for biosignature formation. *ISME J* **5**: 717–727.

Croal L, Johnson C, Beard B & Newman DK (2004) Iron isotope fractionation by Fe (II)-oxidizing photoautotrophic bacteria. *Geochim Cosmochim Acta* **68**: 1227–1242.

Croal L, Jiao Y & Newman DK (2007) The fox operon from *Rhodobacter* strain SW2 promotes phototrophic Fe(II)

oxidation in *Rhodobacter capsulatus* SB1003. *J Bacteriol* **189**: 1774–1782.

Crowe SA, Jones C, Katsev S *et al.* (2008) Photoferrotrophs thrive in an Archean Ocean analogue. *P Natl Acad Sci USA* **105**: 15938–15943.

Czaja AD, Johnson CM, Beard BL, Roden EE, Li W & Moorbath S (2013) Biological Fe oxidation controlled deposition of banded iron formation in the ca. 3770 Ma Isua Supracrustal Belt (West Greenland). *Earth Planet Sci Lett* **363**: 192–203.

Ehrenreich A & Widdel F (1994) Anaerobic oxidation of ferrous iron by purple bacteria, a new type of phototrophic metabolism. *Appl Environ Microbiol* **60**: 4517–4526.

Emerson D & Ghiorse WC (1993) Ultrastructure and chemical composition of the sheath of *Leptothrix discophora* SP-6. *J Bacteriol* **175**: 7808–7818.

Emerson D & Revsbech NP (1994) Investigation of an iron-oxidizing microbial mat community located near Aarhus, Denmark: field studies. *Appl Environ Microbiol* **60**: 4022–4031.

Hallberg R & Ferris FG (2004) Biomineralization by *Gallionella*. *Geomicrobiol J* **21**: 325–330.

Hansel CM, Benner SG, Neiss J, Dohnalkova A, Kukkadapu RK & Fendorf S (2003) Secondary mineralization pathways induced by dissimilatory iron reduction of ferrihydrite under advective flow. *Geochim Cosmochim Acta* **67**: 2977–2992.

Hansel CM, Benner SG, Nico P & Fendorf S (2004) Structural constraints of ferric (hydr)oxides on dissimilatory iron reduction and the fate of Fe(II). *Geochim Cosmochim Acta* **68**: 3217–3229.

Hao L, Li J, Kappler A & Obst M (2013) Mapping of heavy metal ion sorption to cell-mineral aggregates using metal-selective fluorescent probes and CLSM. *Appl Environ Microbiol* **79**: 6524–6534.

Hardie LA (2003) Secular variations in Precambrian seawater chemistry and the timing of Precambrian aragonite seas and calcite seas. *Geology* **31**: 785–788.

Hegler F, Posth N, Jiang J & Kappler A (2008) Physiology of phototrophic iron (II)-oxidizing bacteria: implications for modern and ancient environments. *FEMS Microbiol Ecol* **66**: 250–260.

Hegler F, Schmidt C, Schwarz H & Kappler A (2010) Does a low-pH microenvironment around phototrophic FeII-oxidizing bacteria prevent cell encrustation by FeIII minerals? *FEMS Microbiol Ecol* **74**: 592–600.

Jiao Y & Newman DK (2007) The *pio* operon is essential for phototrophic Fe (II) oxidation in *Rhodopseudomonas palustris* TIE-1. *J Bacteriol* **189**: 1765–1773.

Johnson CM, Beard BL, Beukes NJ, Klein C & O'Leary JM (2003) Ancient geochemical cycling in the Earth as inferred from Fe isotope studies of banded iron formations from the Transvaal Craton. *Contrib Mineral Petrol* **144**: 523–547.

Kappler A & Newman DK (2004) Formation of Fe(III)-minerals by Fe(II)-oxidizing photoautotrophic bacteria. *Geochim Cosmochim Acta* **68**: 1217–1226.

Kappler A, Pasquero C, Konhauser KO & Newman DK (2005a) Deposition of banded iron formations by anoxygenic phototrophic Fe(II)-oxidizing bacteria. *Geology* **33**: 865–868.

Kappler A, Schink B & Newman DK (2005b) Fe(III) mineral formation and cell encrustation by the nitrate-dependent Fe (II)-oxidizer strain BoFeN1. *Geobiology* **3**: 235–245.

Klueglein N, Zeitvogel F, Stierhof YD, Floetenmeyer M, Konhauser KO, Kappler A & Obst M (2014) Potential role of nitrite for abiotic Fe(II) oxidation and cell encrustation during nitrate reduction by denitrifying bacteria. *Appl Environ Microbiol* **80**: 1051–1061.

Koehler I, Konhauser KO, Papineau D, Bekker A & Kappler A (2013) Biological carbon precursor to diagenetic siderite with spherical structures in iron formations. *Nat Commun* **4**: 1741.

Konhauser KO, Hamade T, Raiswell R, Morris RC, Ferris FG, Southam G & Canfield DE (2002) Could bacteria have formed the Precambrian banded iron formations? *Geology* **30**: 1079–1082.

Konhauser KO, Newman DK & Kappler A (2005) The potential significance of microbial Fe(III) reduction during deposition of Precambrian banded iron formations. *Geobiology* **3**: 167–177.

Konhauser KO, Kappler A & Roden EE (2011) Iron in microbial metabolism. *Elements* **7**: 89–93.

Larese-Casanova P, Haderlein SB & Kappler A (2010) Biomineralization of lepidocrocite and goethite by nitrate-reducing Fe(II)-oxidizing bacteria: effect of pH, bicarbonate, phosphate, and humic acids. *Geochim Cosmochim Acta* **74**: 3721–3734.

Maliva RG, Knoll AH & Simonson BM (2005) Secular change in the Precambrian silica cycle: insights from chert petrology. *Geol Soc Am Bull* **117**: 835–845.

Miot J, Benzerara K, Obst M, Kappler A, Hegler F, Schadler S, Bouchez C, Guyot F & Morin G (2009a) Extracellular iron biomineralization by photoautotrophic iron-oxidizing bacteria. *Appl Environ Microbiol* **75**: 5586–5591.

Miot J, Benzerara K, Morin G, Bernard S, Beyssac O, Larquet E, Ona-Nguema G, Kappler A & Guyot F (2009b) Transformation of vivianite by anaerobic nitrate-reducing iron-oxidizing bacteria. *Geobiology* **7**: 373–384.

Overmann J & Garcia-Pichel F (2000) The phototrophic way of life. *The Prokaryotes*, Vol. 2 (Dworkin M, Falkow S, Rosenberg E, Schleifer K-H & Stackebrandt E, eds), pp. 22–85. Springer, New York.

Porsch K & Kappler A (2011) FeII oxidation by molecular O_2 during HCl extraction. *Environ Chem* **8**: 190–197.

Posth NR, Hegler F, Konhauser KO & Kappler A (2008) Alternating Si and Fe deposition caused by temperature fluctuations in Precambrian oceans. *Nat Geosci* **1**: 703–708.

Posth NR, Köhler I, Swanner E, Schröder C, Wellmann E, Binder B, Konhauser KO, Neumann U, Berthold C & Nowak M (2013) Simulating Precambrian banded iron formation diagenesis. *Chem Geol* **362**: 66–73.

Ramesh A, Lee DJ & Hong SG (2006) Soluble microbial products (SMP) and soluble extracellular polymeric substances (EPS) from wastewater sludge. *Appl Microbiol Biotechnol* **73**: 219–225.

Reinhard CT & Planavsky NJ (2011) Mineralogical constraints on Precambrian pCO_2. *Nature* **474**: E1. DOI: 10.1038/nature09959.

Repeta DJ, Simpson DJ, Jorgensen BB & Jannasch HW (1989) Evidence for anoxygenic photosynthesis from the distribution of bacteriochlorophylls in the Black-Sea. *Nature* **342**: 69–72.

Saini G & Chan C (2013) Near-neutral surface charge and hydrophilicity prevent mineral encrustation of Fe-oxidizing micro-organisms. *Geobiology* **11**: 191–200.

Saraiva IH, Newman DK & Louro RO (2012) Functional characterization of the FoxE iron oxidoreductase from the photoferrotroph *Rhodobacter ferrooxidans* SW2. *J Biol Chem* **287**: 25541–25548.

Schaedler S, Burkhardt C, Hegler F, Straub K, Miot J, Benzerara K & Kappler A (2009) Formation of cell-iron-mineral aggregates by phototrophic and nitrate-reducing anaerobic Fe (II)-oxidizing bacteria. *Geomicrobiol J* **26**: 93–103.

Slomp CP, Malschaert JFP, Lohse L & Van Raaphorst W (1997) Iron and manganese cycling in different sedimentary environments on the North Sea continental margin. *Cont Shelf Res* **17**: 1083–1117.

Sobolev D & Roden EE (2001) Suboxic deposition of ferric iron by bacteria in opposing gradients of Fe (II) and oxygen at circumneutral pH. *Appl Environ Microbiol* **67**: 1328–1334.

Stookey L (1970) Ferrozine—a new spectrophotometric reagent for iron. *Anal Chem* **42**: 779–781.

Straub KL, Rainey FA & Widdel F (1999) *Rhodovulum iodosum* sp. nov. and *Rhodovulum robiginosum* sp. nov., two new marine phototrophic ferrous-iron-oxidizing purple bacteria. *Int J Syst Bacteriol* **49**: 729–735.

Swanner ED, Nell RM & Templeton AS (2011) Ralstonia species mediate Fe-oxidation in circumneutral, metal-rich subsurface fluids of Henderson mine, CO. *Chem Geol* **284**: 339–350.

Vargas M, Kashefi K, Blunt-Harris EL & Lovley DR (1998) Microbiological evidence for Fe(III) reduction on early Earth. *Nature* **395**: 65–67.

Weber K, Urrutia M, Churchill P, Kukkadapu R & Roden E (2006) Anaerobic redox cycling of iron by freshwater sediment microorganisms. *Environ Microbiol* **8**: 100–113.

Xiong J (2006) Photosynthesis: what color was its origin. *Genome Biol* **7**: 245.1–245.5.

Xu H, Cai H, Yu G & Jiang H (2013) Insights into extracellular polymeric substances of cyanobacterium *Microcystis aeruginosa* using fractionation procedure and parallel factor analysis. *Water Res* **47**: 2005–2014.

Yang Z, She M, Yin B, Cui J, Zhang Y, Sun W, Li J & Shi Z (2012) Three Rhodamine-based "off–on" Chemosensors with high selectivity and sensitivity for Fe^{3+} imaging in living cells. *J Org Chem* **77**: 1143–1147.